A Novel Mutual Coupling ANN Model for MIMO Antennas With Physical Preprocessing

Yutong Jiang, *Student Member, IEEE*, Shuai S. A. Yuan, and Wei E. I. Sha, *Senior Member, IEEE*

***Abstract*—Mutual coupling model is crucial in designing multiple-input–multiple-output (MIMO) antennas since mutual coupling will degrade overall MIMO performance from distorted radiation patterns and reduced antenna efficiencies. Typically, full-wave simulations have to be employed, which is often time-consuming. Here, the artificial neural network (ANN) method is developed to reduce the modelling time. Compared to previous ANN methods that directly use model parameters as input, a novel physical preprocessing approach is proposed to incorporate antenna correlation information before the network training. As a proof of concept, the mutual coupling model of a nonuniform strongly-coupled array is realized. Furthermore, we use the trained networks for capacity estimation and power allocation with the water-filling algorithm, showing favorable model performance. The proposed physically preprocessed ANN model significantly outperforms traditional analytical solutions and direct modelling networks in terms of prediction accuracy, dataset construction costs, and network convergence, which could facilitate the fast optimization and design of advanced antenna arrays for MIMO communications.**

***Index Terms*—Artificial neural network (ANN), capacity-aimed optimization, mutual coupling, nonuniform multiple-input–multiple-output (MIMO) antennas, physical preprocessing.**

I. Introduction

MULTIPLE-input–multiple-output (MIMO) technology is critical in 5G wireless communication systems as an enabler that provides the degree-of-freedom and power gains, thus the capacity gains [1], [2], [3], [4], [5], [6]. Traditionally, by leveraging physical parameters, such as array element sizes or positions to calculate analytical radiation patterns and efficiency limits, we can harness MIMO technology for advanced functions, such as beamforming [7], [8], channel estimation, and spatial multiplexing [9], [10]. However, when optimizing MIMO performance, mutual coupling is unavoidable, which causes severe performance degradation. For a given coupled antenna array (CAA) system, both the degree of freedom and signal-to-noise ratio (SNR) of a MIMO system are affected by the mutual coupling since the distorted embedded radiation patterns will change the correlations between elements, and the power coupling will reduce radiation efficiency [11], [12], [13], [14]. The analytical calculations result in unacceptable errors (due to the physical symmetry breaking), especially for nonuniform arrays, affecting subsequent applications. In addition, traditional antenna array optimization metrics, such as gain and directivity, may not lead to improved communication performance (capacity) [15], [16].

Ground truth values considering mutual coupling can be obtained through full-wave simulation, but the iterative solving process usually takes a great amount of simulation time, posing a fatal drawback when implementing optimization methods. Recently, researchers have widely adopted machine learning methods, such as artificial neural networks (ANNs) for coupling compensation [17], [18], coupling modeling [19], [20], coupling prediction or decoupling to solve such problems [21], [22], [23], [24], [25], [26]. Although the training (learning) process is time-consuming, once trained, these networks can solve problems while satisfying the current requirements of millisecond response time. However, previous works often use ANNs to extract relatively general information [27], [28], such as directly using physical parameters as inputs to train the network for obtaining output targets. These approaches suffer from a common issue: as the topological complexity of the CAA increases, the network needs a larger number of training datasets to establish the complex mapping relation, which increases the difficulty of dataset and network construction. Moreover, few pieces of literature establish a model linking topology to the ultimate communication performance for antenna array optimization [29], [30], [31].

In this letter, physical principles governing antenna correlation inspire us to propose an ANN method consisting of calculated physical parameters (approximate values) [32], [33] as input and simulation results (ground-truth values) as output. In this article, mainly two contributions are made as follows.

1) First, with a millisecond response time, we use ANN to fully consider the mutual coupling effects of nonuniform tightly CAA, as a proof of concept, which are more accurate than analytical solutions and faster than full-wave simulations. Using the predicted values, we can acquire the optimal MIMO capacity. For emerging nonuniform and holographic arrays [34], [35], [36], even with the best antenna design, the coupling cannot be avoided. The surrogate model from topology to capacity facilitates array optimization with a focus on enhancing communication performance.
2) Furthermore, by introducing the physical preprocessing, the approximate parameter values are used as input to map the ground truth values of the same physical parameters.

Received 9 August 2024; accepted 30 August 2024. Date of publication 6 September 2024; date of current version 13 December 2024. *(Corresponding author: Wei E. I. Sha.)*

The authors are with the College of Information Science and Electronic Engineering, Zhejiang University, Hangzhou 310027, China (e-mail: ytjiang@zju.edu.cn; weisha@zju.edu.cn).

Digital Object Identifier 10.1109/LAWP.2024.3454336

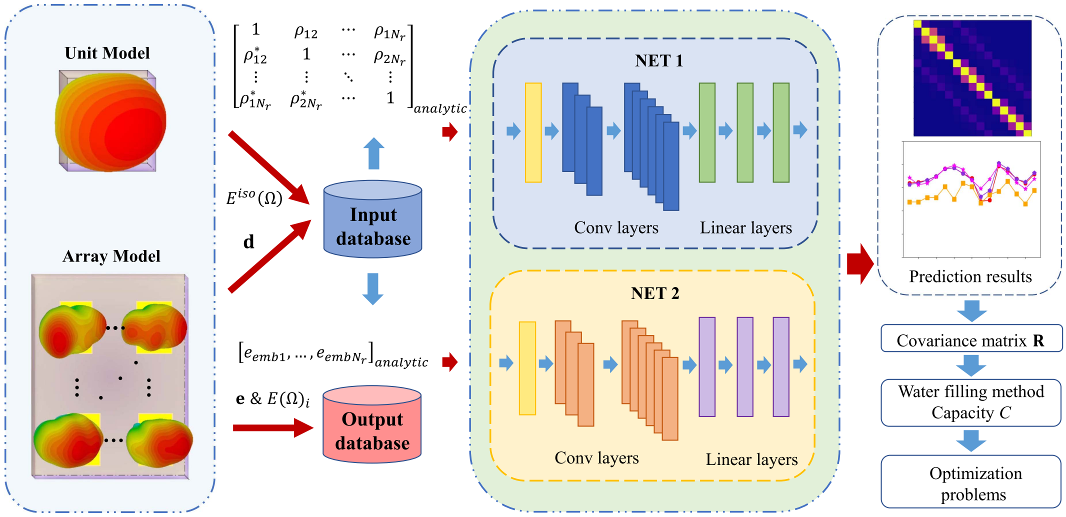

Fig. 1. Workflow of power allocation and capacity estimation by the physically preprocessed ANNs includes four parts. Part 1: CAA model construction. We employ thousands of full-wave simulations to obtain the distance vectors, efficiency vectors and active radiation patterns. Part 2: dataset construction. We calculate analytical correlation matrices and efficiency vectors as parts of datasets. Part 3: network construction and training. We train NET1 and NET2 to obtain predicted correlation matrices and efficiency vectors. Part 4: results calculation and analysis. We use the predicted values to estimate the capacity of the channel.

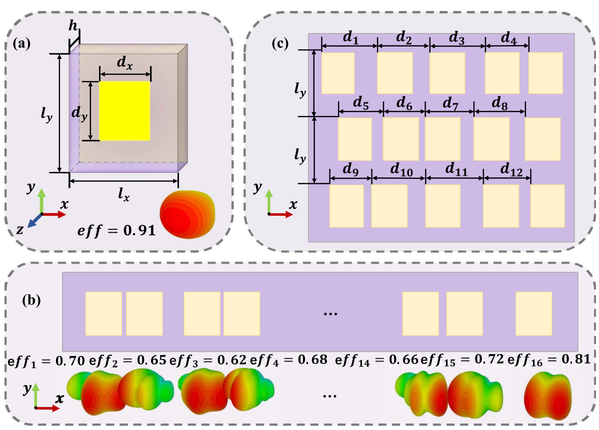

Fig. 2. CAA model. (a) Microstrip antenna element. The substrate material is FR-4. $d_x = 28$ mm, $l_x = 0.45\lambda$, $d_y = 0.5 \times l_y = 37.26$ mm, $h = 3$ mm, and the working frequency is 2.45 GHz. (b) Nonuniform 16 × 1 1D array model. (c) Nonuniform 5 × 3 2S array model.

It is the first time we have realized power allocation and capacity estimation by using the physically preprocessed ANNs.

II. Principle and Method

The basic idea of our work is shown in Fig. 1, which could be generally divided into the following four parts.

A. CAA Model

First, we construct the CAA model to obtain training datasets. We use a typical microstrip antenna element for convenience, as shown in Fig. 2(a). The antenna element includes three layers: the top layer of the patch, the middle layer of the substrate and the bottom layer of the ground. Each antenna is fed from underneath via a coaxial probe. We perform simulations using the commercial software CST. The simulation result shows that the S_{11} of the antenna element at the working frequency is -16.2 dB, and the total efficiency is 0.91. Fig. 2(b) and (c) shows the 1-D and 2-D MIMO array models. There are N_x patches along the x-direction and N_y patches along the y-direction. The spacing in the y-direction is fixed to l_y, and the spacing in the x-direction is $d_i \in \mathbf{d}$, which is randomly valued between 0.25λ and 0.45λ (λ is the free-space wavelength). The boundary conditions in all directions are opened. Observing the active element patterns in Fig. 2, we can find the patterns are severely distorted, and the efficiencies are decreased, which proves that the coupling effect is significant.

B. Channel Model

$\mathbf{R}$ is the covariance matrix of the antenna array, which is a function of the correlation matrix $\mathbf{\Phi}$ and the efficiency matrix $\mathbf{\Xi}$ according to [37]

$$\mathbf{R} = \mathbf{\Phi} \circ \mathbf{\Xi} \tag{1}$$

where $\circ$ is the entry-wise product. Assuming that there are N antennas, the correlation matrix incorporating mutual coupling is

$$\mathbf{\Phi} = \begin{bmatrix} 1 & \rho_{12} & \cdots & \rho_{1N} \\ \rho_{21}^* & 1 & \cdots & \rho_{2N} \\ \vdots & \vdots & \ddots & \vdots \\ \rho_{N1}^* & \rho_{N2}^* & \cdots & 1 \end{bmatrix} \tag{2}$$

where ρ_{ij} could be calculated using embedded radiation patterns $E(\Omega)$[11], and the embedded efficiency matrix Ξ is expressed by

$$\Xi = \sqrt{\mathbf{e}}\sqrt{\mathbf{e}}^T \tag{3}$$

with $\mathbf{e} = [e_{\text{emb}1}, e_{\text{emb}2}, \ldots, e_{\text{emb}N}]^T$, the embedded radiation efficiency of the nth antenna could be calculated by S-parameters assuming negligible ohmic loss [11].

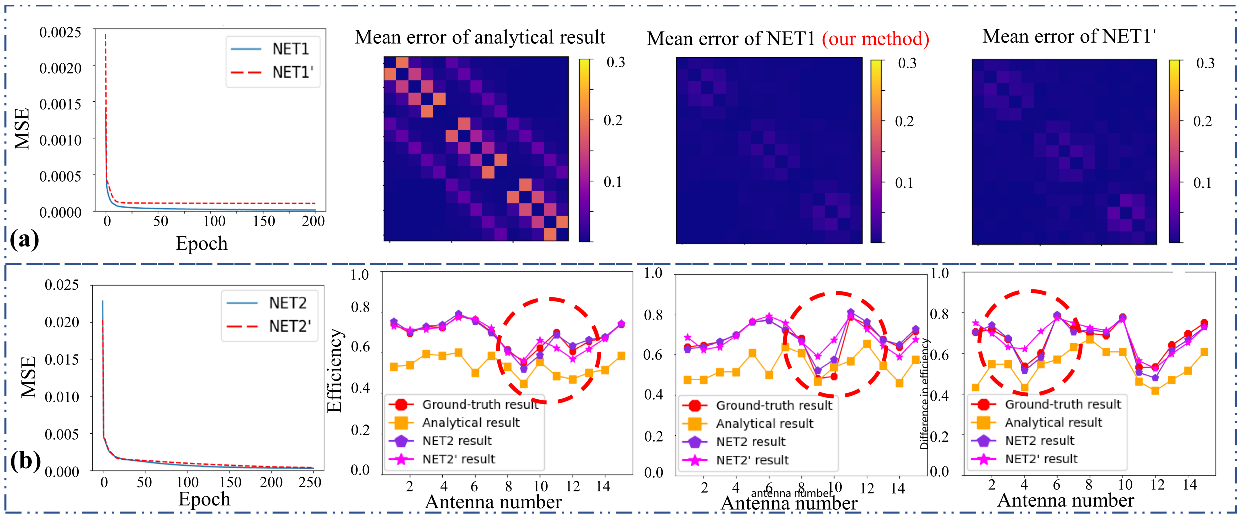

Fig. 3. Network training results. (a) Results for the covariance matrix. The MSE decreases with the increase of epoch. The mean error matrices (the same size as the covariance matrix) of the analytical method, NET1 method and NET1′ method, compared to simulation results (ground truth). (b) Results for efficiency vector. The MSE decreases with the increase of epoch. Three cases were calculated using the analytical method, NET2 method and NET2′ method, compared to simulation results (ground truth).

TABLE I
NETWORKS' PARAMETERS

Para. / Net.	Input	Output	Notes
NET1	$\mathbf{\Phi}'$	$\mathbf{\Phi}$	**our method**
NET1′	$\mathbf{d}$	$\mathbf{\Phi}$	a network compared to NET1
NET2	$\mathbf{\Xi}'$	$\mathbf{\Xi}$	**our method**
NET2′	$\mathbf{d}$	$\mathbf{\Xi}$	a network compared to NET2
NET3	$\mathbf{d}$	λ_i	a network compared to our method in water-filling power allocation

Without considering the mutual coupling, we could approximately calculate the corresponding analytical parameters with their analytical forms. The analytical embedded radiation pattern of the nth antenna is [38]

$$E(\Omega)' = E^{\mathrm{iso}}(\Omega) \exp\left(j\mathbf{k}_\Omega \cdot \boldsymbol{r}_n\right) \tag{4}$$

where $\boldsymbol{k}_\Omega$ is the wave vector and r_n is the position of the nth antenna. According to Hannan's limit [32], the analytical embedded antenna efficiency of the nth antenna is

$$e'_{\mathrm{embn}} = \frac{\pi S_n}{\lambda^2} \tag{5}$$

where S_n is the elementary area of the nth antenna element.

C. Network model

We build five networks, including our method and the compared networks. The differences among them are given in Table I, where $\mathbf{\Phi}'$ and $\mathbf{\Xi}'$ represent the analytical values.

Generally, the most crucial difference is the inputs. Physical preprocessing is introduced compared to commonly used direct networks. Moreover, we also set up NET3, which serves as the commonly used direct prediction model. We use CNNs, which feature two convolutional layers and three linear layers. Except for these above, all the networks possess the same construction for fair comparison. The first layer uses 30 filters of size 3×3 with a stride of 1 to maintain the input size. The second layer increases the number of filters to 60, using the same filter size, which helps capture more complex features. Each convolutional layer is followed by a rectified linear unit activation function. Following each convolutional layer, a max pooling layer with a 2×2 window and a stride of two is used. Linear layers with appropriately sized cells output correctly sized predicted values. We use the Adam optimizer with a learning rate of 0.005. The loss functions for networks are defined as the mean square error (MSE).

D. Capacity Estimation Model

We use the water-filling algorithm [39] for power allocation and calculate the channel capacity. The channel capacity, in this case, can be calculated by [11], [14], [40]

$$\max_P C = E\left\{\sum_{i=1}^{N} \log_2\left(1 + \frac{P_i}{\sigma^2} \times \lambda_i\right)\right\} \tag{6}$$

where E denotes the ensemble average, N represents the antenna number, σ^2 represents the noise power, P_i represents the power allocated to the ith antenna, which is calculated using the water-filling algorithm based on λ_i, λ_i represents the eigenvalues of $\mathbf{R}\mathbf{H}_w\mathbf{H}_w^\dagger$ and $\mathbf{H}_w$ denotes the spatially white MIMO channel with independent identically distributed complex Gaussian entries, simulating the fluctuations of a Rayleigh channel.

III. RESULTS AND DISCUSSION

We obtain the active element radiation patterns and the efficiencies of the antenna element of 1200 groups of 5×3 sized randomly arranged nonuniform arrays. In total, 70% of them are the training datasets, and the rest are the test datasets.

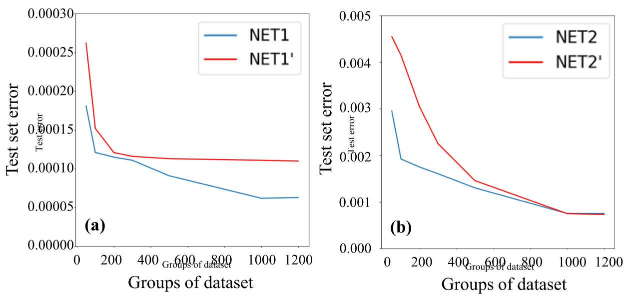

Fig. 4. Test errors under different dataset sizes. When the group number of the dataset is smaller than 1200, the dataset is randomly chosen from the original 1200-sized datasets, and the test set error is tested several times and averaged to ensure stability. (a) Results for NET1 and NET1′. (b) Results for NET2 and NET2′.

A. Network Training Result

Fig. 3 presents the results of the correlation matrix $\mathbf{\Phi}$ and the efficiency vector $\mathbf{e}$, respectively. For NET1 and NET1′ in (a), due to the incorporation of physical information, NET1 converges faster than NET1′. The mean error between the analytical result and the ground truth result is significantly larger than that of NET1 and NET1′, highlighting the superior performance of the ANNs. The average MSEs of test datasets of NET1 and NET1′ are 6.3e−5 and 1.1e−4, respectively. The comparison of the mean error of NET1 and NET1′ also reveals that NET1 performs better, which is an advantage provided by physical preprocessing.

Similarly, For NET2 and NET2′ in (b), the predicted values of NET2 and NET2′ are remarkably close to the ground truth values. The average MSEs of test datasets are 7.7e−4 and 7.5e−4, respectively. Despite similar average MSEs, NET2 outperforms NET2′ in cases where an element's efficiency significantly differs from its neighbors, as illustrated by the red circles, demonstrating the benefit of physical preprocessing. Using NET2, 93.8% of efficiency errors in the test sets cluster between −0.05 and 0.05, compared to 83.4% using NET2′. However, the efficiency values calculated by Hannan's limit are generally smaller than the ground truth, primarily due to our array being small and nonuniform, and thus strongly affected by edge effects [41].

We also examined the networks' learning efficiency using different sizes of training datasets, as shown in Fig. 4. In Fig. 4(a), NET1 performs better than NET1′ in the dataset of all the tested sizes. In Fig. 4(b), NET2 performs better than NET2′ when the dataset size is less than 1000. Increasing the training dataset or model complexity may lower test error but at the cost of more time and resources, yet our method's error already meets engineering standards. The physical preprocessing simplifies the features our network needs to learn, especially for networks with complex mappings, thereby requiring fewer datasets to achieve comparable training results and reducing the cost of dataset construction.

B. Capacity Estimation Results

Fig. 5(a) is a schematic diagram of water-filling using different methods. The blue line is inversely proportional to the channel

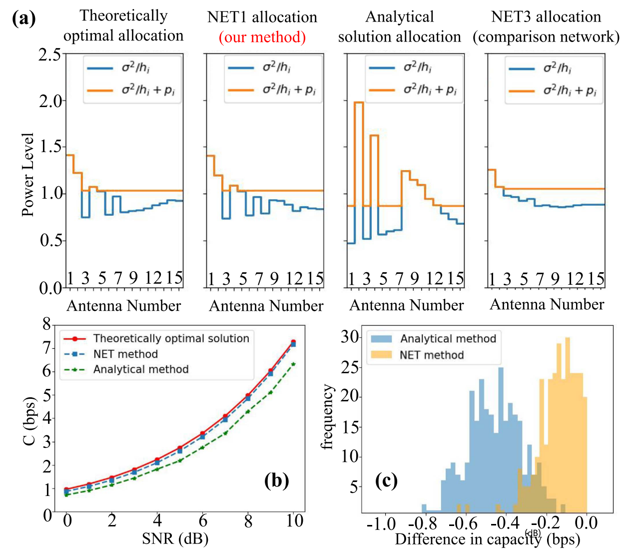

Fig. 5. Capacity estimation results. (a) Power allocation using four different methods. (b) Channel capacity using corresponding power allocation under different SNR conditions. The blue dot line represents the results of our method. (c) Frequency distribution histogram of the error between the analytical result and our method result relative to the theoretically optimal solution.

quality, and the difference between the orange and blue lines represents the allocated power of the channel. The channel quality predicted by our method closely matches that calculated from full-wave simulation (the theoretically optimal allocation). However, the analytical solution and NET3 allocation both result in significant estimation errors in channel quality, leading to poor power distribution. Furthermore, while full-wave simulation requires 40 min to 90 min for a randomly constructed 5×3 sized nonuniform CAA, our trained neural network achieves capacity estimation within 50 ms. Fig. 5(b) illustrates the impact of different methods on channel capacity estimation under different SNR conditions, with our method (blue line) approaching the theoretically optimal channel capacity. Fig. 5(c) is a statistical graph comparing the error between our neural network and the analytical method for 300 test sets against the theoretically optimal channel capacity. Instances of poor performance are uncommon using our approach, indicating the high resilience of our model.

IV. Conclusion

We developed a novel ANN model that improves capacity estimation accuracy by incorporating mutual coupling through physical preprocessing. This model excels particularly with nonuniform CAA, outdoing traditional analytical methods and commonly used direct prediction models. It reduces dataset costs, accelerates network convergence, and illustrates the benefits of integrating physical information with machine learning for advancing communication system design and evaluation, making it a promising candidate for further antenna array optimization. Future research will investigate the model's capability to be applied to various scales and types of antenna arrays and array optimization.

REFERENCES

[1] K. Dovelos, M. Matthaiou, H. Q. Ngo, and B. Bellalta, "Channel estimation and hybrid combining for wideband terahertz massive MIMO systems," *IEEE J. Sel. Areas Commun.*, vol. 39, no. 6, pp. 1604–1620, Jun. 2021.

[2] D. Tse and P. Viswanath, *Fundamentals of Wireless Communication*. Cambridge, U.K.: Cambridge Univ. Press, 2005.

[3] G. Oliveri, G. Gottardi, N. Anselmi, and A. Massa, "Capacity-driven low-interference fast beam synthesis for next generation base stations," *IEEE Trans. Antennas Propag.*, vol. 70, no. 6, pp. 4472–4484, Jun. 2022.

[4] W. Tang et al., "MIMO transmission through reconfigurable intelligent surface: System design, analysis, and implementation," *IEEE J. Sel. Areas Commun.*, vol. 38, no. 11, pp. 2683–2699, Nov. 2020.

[5] S. S. A. Yuan, Z. He, X. Chen, C. Huang, and W. E. I. Sha, "Electromagnetic effective degree of freedom of a MIMO system in free space," *IEEE Antennas Wireless Propag. Lett.*, vol. 21, no. 3, pp. 446–450, Mar. 2022.

[6] X. Bai, R. Li, S. Tan, S. Mikki, and E. Li, "An electromagnetic analysis of the impact of random scattering and RISs on the shannon capacity of MIMO communication systems," *IEEE Antennas Wireless Propagat. Lett.*, vol. 23, no. 4, pp. 1176–1180, Apr. 2024.

[7] F. Gao, B. Wang, C. Xing, J. An, and G. Y. Li, "Wideband beamforming for hybrid massive MIMO terahertz communications," *IEEE J. Sel. Areas Commun.*, vol. 39, no. 6, pp. 1725–1740, Jun. 2021.

[8] B. Ning et al., "Beamforming technologies for ultra-massive MIMO in terahertz communications," *IEEE Open J. Commun. Soc.*, vol. 4, pp. 614–658, 2023.

[9] Y. Han, S. Jin, C.-K. Wen, and X. Ma, "Channel estimation for extremely large-scale massive MIMO systems," *IEEE Wireless Commun. Lett.*, vol. 9, no. 5, pp. 633–637, May 2020.

[10] G. Bartoli, A. Abrardo, N. Decarli, D. Dardari, and M. Di Renzo, "Spatial multiplexing in near field MIMO channels with reconfigurable intelligent surfaces," *Signal Process.*, vol. 17, no. 3, 2023, Art. no. e12195.

[11] S. S. A. Yuan, X. Chen, C. Huang, and W. E. I. Sha, "Effects of mutual coupling on degree of freedom and antenna efficiency in holographic MIMO communications," *IEEE Open J. Antennas Propag.*, vol. 4, pp. 237–244, 2023.

[12] X. Chen, S. Zhang, and Q. Li, "A review of mutual coupling in MIMO systems," *IEEE Access*, vol. 6, pp. 24706–24719, 2018.

[13] J. W. Wallace and M. A. Jensen, "Mutual coupling in MIMO wireless systems: A rigorous network theory analysis," *IEEE Trans. Wireless Commun.*, vol. 3, no. 4, pp. 1317–1325, Jul. 2004.

[14] K.-H. Chen and J.-F. Kiang, "Effect of mutual coupling on the channel capacity of MIMO systems," *IEEE Trans. Veh. Technol.*, vol. 65, no. 1, pp. 398–403, Jan. 2016.

[15] Y.-X. Zhang, Y.-C. Jiao, and L. Zhang, "Antenna array directivity maximization with sidelobe level constraints using convex optimization," *IEEE Trans. Antennas Propag.*, vol. 69, no. 4, pp. 2041–2052, Apr. 2021.

[16] S. Liang, Z. Fang, G. Sun, Y. Liu, G. Qu, and Y. Zhang, "Sidelobe reductions of antenna arrays via an improved chicken swarm optimization approach," *IEEE Access*, vol. 8, pp. 37664–37683, 2020.

[17] A. M. Alzahed, S. M. Mikki, and Y. M. Antar, "Nonlinear mutual coupling compensation operator design using a novel electromagnetic machine learning paradigm," *IEEE Antennas Wireless Propag. Lett.*, vol. 18, no. 5, pp. 861–865, May 2019.

[18] T. Zhang, Y. Lu, and H. Hui, "Compensation for the mutual coupling effect in uniform circular arrays for 2D DOA estimations employing the maximum likelihood technique," *IEEE Trans. Aerosp. Electron. Syst.*, vol. 44, no. 3, pp. 1215–1221, 2008.

[19] O. J. Famoriji, O. Y. Ogundepo, and X. Qi, "An intelligent deep learning-based direction-of-arrival estimation scheme using spherical antenna array with unknown mutual coupling," *IEEE Access*, vol. 8, pp. 179259–179271, 2020.

[20] O. J. Famoriji and T. Shongwe, "Electromagnetic machine learning for estimation and mitigation of mutual coupling in strongly coupled arrays," *ICT Exp.*, vol. 9, no. 1, pp. 8–15, 2023.

[21] Q. Wu, H. Wang, and W. Hong, "Multistage collaborative machine learning and its application to antenna modeling and optimization," *IEEE Trans. Antennas Propag.*, vol. 68, no. 5, pp. 3397–3409, 2020.

[22] S. Roy and U. Chakraborty, "Mutual coupling reduction in a multi-band MIMO antenna using meta-inspired decoupling network," *Wireless Pers. Commun.*, vol. 114, no. 4, pp. 3231–3246, 2020.

[23] H. Huang, X.-S. Yang, and B.-Z. Wang, "Machine learning-based generative optimization method and its application to antenna decoupling design," *IEEE Trans. Antennas Propag.*, vol. 71, no. 7, pp. 6243–6248, Jul. 2023.

[24] Z. Wei et al., "Fully automated design method based on reinforcement learning and surrogate modeling for antenna array decoupling," *IEEE Trans. Antennas Propag.*, vol. 71, no. 1, pp. 660–671, Jan. 2023.

[25] S. Roshani et al., "Mutual coupling reduction in antenna arrays using artificial intelligence approach and inverse neural network surrogates," *Sensors*, vol. 23, no. 16, 2023, Art. no. 7089.

[26] B. Qian, X. Huang, X. Chen, M. Abdullah, L. Zhao, and A. A. Kishk, "Surrogate-assisted defected ground structure design for reducing mutual coupling in 2× 2 microstrip antenna array," *IEEE Antennas Wireless Propag. Lett.*, vol. 21, no. 2, pp. 351–355, Feb. 2022.

[27] S. Koziel and M. Abdullah, "Machine-learning-powered EM-based framework for efficient and reliable design of low scattering metasurfaces," *IEEE Trans. Microw. Theory Techn.*, vol. 69, no. 4, pp. 2028–2041, Apr. 2021.

[28] M. Abdullah and S. Koziel, "Supervised-learning-based development of multibit RCS-reduced coding metasurfaces," *IEEE Trans. Microw. Theory Techn.*, vol. 70, no. 1, pp. 264–274, Jan. 2022.

[29] W.-C. Weng, F. Yang, and A. Z. Elsherbeni, "Linear antenna array synthesis using Taguchi's method: A novel optimization technique in electromagnetics," *IEEE Trans. Antennas Propag.*, vol. 55, no. 3, pp. 723–730, Mar. 2007.

[30] A. Darvish and A. Ebrahimzadeh, "Improved fruit-fly optimization algorithm and its applications in antenna arrays synthesis," *IEEE Trans. Antennas Propag.*, vol. 66, no. 4, pp. 1756–1766, Apr. 2018.

[31] G. G. Roy, S. Das, P. Chakraborty, and P. N. Suganthan, "Design of non-uniform circular antenna arrays using a modified invasive weed optimization algorithm," *IEEE Trans. Antennas Propag.*, vol. 59, no. 1, pp. 110–118, Jan. 2011.

[32] P. Hannan, "The element-gain paradox for a phased-array antenna," *IEEE Trans. Antennas Propag.*, vol. AP-12, no. 4, pp. 423–433, Jul. 1964.

[33] X. Chen and S. Zhang, "Multiplexing efficiency for MIMO antenna-channel impairment characterisation in realistic multipath environments," *Microw., Antennas Propag.*, vol. 11, no. 4, pp. 524–528, 2017.

[34] T. Gong et al., "Holographic MIMO communications: Theoretical foundations, enabling technologies, and future directions," *IEEE Commun. Surveys Tuts.*, vol. 26, no. 1, pp. 196–257, Firstquarter 2024.

[35] S. S. A. Yuan et al., "Breaking the degrees-of-freedom limit of holographic MIMO communications: A 3D antenna array topology," *IEEE Trans. Veh. Technol.*, vol. 73, no. 8, pp. 11276–11288, Aug. 2024.

[36] E. Anarakifirooz and S. Loyka, "Structural design of non-uniform linear arrays for favorable propagation in massive MIMO," *IEEE Commun. Lett.*, vol. 27, no. 1, pp. 367–371, Jan. 2023.

[37] M. T. Ivrlac and J. A. Nossek, "Diversity and correlation in rayleigh fading MIMO channels," in *Proc. IEEE 61st Veh. Technol. Conf.*, 2005, vol. 1, pp. 151–155.

[38] J. A. Kong et al., "Electromagnetic wave theory and applications," Res. Lab. Electron., Massachusetts Inst. Technol., Cambridge, MA, USA, Progress Rep. 138, 1995.

[39] S. P. Boyd and L. Vandenberghe, *Convex Optimization*. Cambridge, U.K.: Cambridge Univ. Press, 2004.

[40] X. Chen, P.-S. Kildal, J. Carlsson, and J. Yang, "MRC diversity and MIMO capacity evaluations of multi-port antennas using reverberation chamber and anechoic chamber," *IEEE Trans. Antennas Propag.*, vol. 61, no. 2, pp. 917–926, Feb. 2013.

[41] P.-S. Kildal, *Foundations of Antenna Engineering: A Unified Approach for Line-of-Sight and Multipath*. Boston, MA, USA: Artech House, 2015.